Structure, characterization, and properties of BaMoO4 and BaKYb(MoO4)3 flux-grown single-crystals

Monique Tillard, D. Granier, C. Reibel, L. Daenens, P. Armand

Structure, characterization, and properties of $BaMoO_4$ and $BaKYb(MoO_4)_3$ flux-grown single-crystals

M. Tillard, D. Granier, C. Reibel, L. Daenens, P. Armand*

ICGM, Univ Montpellier, CNRS, ENSCM, Montpellier, France

*Corresponding author: pascale.armand@umontpellier.fr

ORCID: P. Armand 0000-0001-8921-5427

M. Tillard 0000-0002-0609-7224

Abstract

Crystals of the barium molybdates $BaKYb(MoO_4)_3$ and $BaMoO_4$ were obtained by spontaneous nucleation from high-temperature flux experiments. The compounds were characterized by energy-dispersive spectrometry (EDS) and Raman spectroscopy, and their structure was solved from single-crystal X-ray diffraction data at room temperature. $BaMoO_4$ crystallizes in the tetragonal $I4_1/a$ symmetry with $a = b = 5.5723(4)$ and $c = 12.7954(9)$ Å. With the scheelite-type structure, $BaMoO_4$ displays sharp and intense lines in its FT-Raman spectrum registered at room temperature. The new triple molybdate $BaKYb(MoO_4)_3$ is described in a monoclinic lattice $C2/c$ of parameters $a = 17.3517(5)$, $b = 12.1477(4)$, $c = 5.2481(2)$ Å, $\beta = 105.344(2)°$. The Yb^{3+} ions are surrounded by oxygen leading to YbO_8 coordination polyhedra while atomic disorder is observed for the cations Ba^{2+} and K^+, statistically sharing their positions inside 8-vertex coordination polyhedra. The Raman spectrum confirms the presence of distorted MoO_4 tetrahedra for the $BaKYb(MoO_4)_3$ molybdate. Investigation of its magnetic properties was undertaken in order to check whether a magnetic ordering occurs at low temperature.

Keywords: Molybdate, Crystal structure, Raman investigation; Magnetic susceptibility

1. Introduction

Simple molybdates with the general formula *Me*MoO_4 (*Me*$^{2+}$ = Ba, Sr, Ca, Pb) and the scheelite-like structure are potential stimulated Raman scattering (SRS) materials and promising hosts for the incorporation of optically active ions [1-3]. On the other hand, double molybdates of general formula *ALn*MoO_4 (A^+ = alkaline metals, Cu or Tl) have received considerable attention due to their amazing properties and their thermal and chemical stability [4-10]. They have a high potential application in various fields, such as lanthanide (*Ln*) luminescence [5-6], Li-ion or Na-ion batteries [7, 8], and laser hosts activated by Ln^{3+} ions [9, 10]. Yb^{3+}-doped solid state lasers with large ground state $^2F_{7/2}$ splitting through strong crystal field effects (CF) are interesting alternatives to those based on Nd^{3+} as large homogeneous spectral broadening and larger laser gain bandwidths could be reached [11]. Since CF effects are dependent on the structural characteristics of the lanthanide site in the crystal network, the search for new materials with a multisite Yb^{3+} occupation and highly distorted coordination polyhedra around Yb^{3+} has generated a lot of interest. The results presented in the current paper have been obtained in the course of a more general study aimed at the synthesis and structural evaluation of Yb-based magnetically-concentrated double molybdates more recently described [12, 13]. $KYb(MoO_4)_2$ crystallizes in the orthorhombic symmetry, space group P*bcn* (No. 60), with a complete ordering of the Yb^{3+} and Mo^{6+} cations [12]. The Yb^{3+} ions are located in distorted YbO_8 antiprisms which form chains, by sharing edges, aligned along the *c*-axis. $LiYbMo_2O_8$ displays the tetragonal symmetry and is described in the noncentrosymmetric $I\bar{4}$ space group (No. 82) [13] with an atomic local disorder as Li^+ and Yb^{3+} cations share their sites inside regular MO_8 dodeca-deltahedra (*M* = Li/Yb).

The high-temperature synthesis of $BaMoO_4$ and $BaKYb(MoO_4)_3$, grown from the solution as millimeter-sized single crystals, is described. Besides, the monoclinic structure of the new molybdate $BaKYb(MoO_4)_3$ is provided with also a structural determination from crystal

diffraction of the tetragonal $BaMoO_4$ scheelite-like structure. The room temperature structural study is completed by vibrational characterizations via Raman spectroscopy. The magnetic properties of the ternary molybdate are presented with both the temperature-dependent susceptibility and the field-dependent magnetization recorded from 1.8 to 300 K.

2. Experimental

2.1. Materials preparation

The flux growth was carried out by the slow-cooling method with spontaneous nucleation. $Ba_3Yb_4O_9$ was chosen as the solute as we already synthesized this pure phase for previous works, and K_2CO_3 (or Rb_2CO_3)-$3MoO_3$ mixtures as the fluxes (solvents). All the starting reagents are high purity Alfa Aesar commercial products, MoO_3 (99.95%), Yb_2O_3 (99.9%), $BaCO_3$ (99%), K_2CO_3 (99%), Rb_2CO_3 (99%), and were used as received. $Ba_3Yb_4O_9$ was synthesized via a solid-state reaction from $3BaCO_3$ and $2Yb_2O_3$ heated at 1400 °C during 12 hours in the air (see Supplementary Materials S.1). The K_2CO_3-$3MoO_3$ mixture (or Rb_2CO_3-$3MoO_3$) was heated in air at 520 °C for at least 8 days. This step allowed to get high quantities of $K_2Mo_3O_{10}$ or $Rb_2Mo_3O_{10}$ compounds in the powder form. We did not tried to use the self-flux method consisting to directly prepare the compound by heating a stoichiometric mixture of all the required oxides, as for example K_2O-BaO-Yb_2O_3 and MoO_3.

The solute/flux powders, $Ba_3Yb_4O_9$ and K_2CO_3-$3MoO_3$ (or Rb_2CO_3-$3MoO_3$) were mixed in 10/90 weight proportions and an amount of 20 g of powder was loaded into a Pt crucible covered with a lid. This solute + flux mixture was heated in a resistance-heated furnace at 970 °C for 3 hours in the air to ensure a good dissolution of the solute. The complete dissolution of the solute in the flux has not been specially monitored or measured. After that, the sample was cooled by decreasing first the temperature to 600 °C at the rate of 0.9 °/h, and next to room temperature at 200 °/h.

2.2. Materials characterization

The materials obtained as individualized colorless crystals were characterized by classical analyses such as EDX, Raman spectroscopy, and X-ray diffraction. Their chemical composition was obtained by Energy Dispersive X-ray spectroscopy on a Quanta 200 FEG (FEI) scanning electron microscope equipped with an SDD diode detector (Oxford INCA). The spectra were recorded under a primary vacuum (around 10^{-5} Torr) at a voltage of 15 kV. To control the quality/homogeneity of the crystals, at least three zones were probed for each sample.

2.3. X-ray diffraction

A stereo microscope equipped with a polarizing filter was used to select single colorless and faceted crystals suitable for X-ray diffraction data collection (Mo Kα radiation, room temperature) either using an Xcalibur CCD (Oxford diffraction) or a Bruker D8 Venture diffractometer. The appropriate software suites CrysAlis [14] or Apex [15] were used for the treatment of data, the Lorentz-polarization, and absorption corrections. The structures were solved and refined using the SHELX programs [16, 17] and anisotropic displacement parameters were considered for all atoms in full-matrix least-squares refinements on F^2. The entire filling of the sites was checked by the free refinement of site occupation factors. Structural representations have been drawn using the program Diamond [18].

2.4. Raman measurements

Unpolarized Raman spectra were recorded at room temperature on a LabRam Aramis spectrometer (Horiba Jobin-Yvon) at the He-Ne wavelength (λ = 632.8 nm). This device is equipped with a CCD detector cooled by the Peltier effect and a motorized stage. According to

the instrumental error of 1 cm^{-1} on the measurement, the frequencies of Raman vibration modes in wavenumber, are given to within one unit.

2.5. Magnetic measurements

Magnetic measurements were carried out using a commercial Superconducting Quantum Interference Device (SQUID) MPMS-7XL magnetometer in DC mode, allowing to explore the temperature range of 1.8 - 300 K with H external magnetic fields ranging from 0 to 5 Tesla with a sensitivity of the order of 10^{-8} emu. A powdered sample of $BaKYb(MoO_4)_3$ of 63.6 mg was weighed and placed in a capsule introduced in a plastic straw. The negligible diamagnetic contribution of the straw has not been subtracted from our data.

3. Results and discussion

3.1. Growth of crystals

At the end of each high temperature flux growth experiment, the solidified mixture was dissolved in water, and numerous colorless and transparent crystals spontaneously grown (0.2-2 mm in size) were isolated. No post-growth annealing was applied.

In case of use of the K-based flux, two kinds of single-crystals were obtained with a growth yield of about 20%. Plate-like as-grown crystals with the $KYb(MoO_4)_2$ composition [12], and bulky and well-faceted crystals with no inclusion visible to the eyes (Supporting information Figure S2). The EDX analyses have confirmed the formula $BaKYb(MoO_4)_3$ giving an atomic ratio Ba:K:Yb:Mo:O of 1.1(1):1.1(1):0.9(1):3:12(1) with no significant variation in chemical composition when scanning across the raw surface of the crystal. When using the Rb-based flux for the growth experiment, only one kind of single-crystals with under-millimeter size was obtained with a yield of about 5 %. The EDX analysis indicated that neither Rb nor Yb entered into the compound composition, leading to the barium molybdate $BaMoO_4$.

3.2. Single-crystal structure of $BaMoO_4$

The single-crystal structure of $BaMoO_4$ refined in the tetragonal space group $I4_1/a$ to a final agreement factor R1 of 1.28% is in very good agreement with the previous works mentioned in the Pearson Crystal structure database [19] among which, only one, with R1 = 14%, refers to a single-crystal refinement [20]. It also closely matches the most recent and accurate structural determination undertaken on a nanosized polycrystalline sample using synchrotron data [21].

The structural model includes Mo at 4*a*, Ba at 4*b* and O at 16*f* positions. Regular MoO_4 tetrahedra ($\bar{4}$ symmetry) are characterized by 4 × Mo-O distances of 1.761(1) Å with 4 × 108.2(1) and 2 × 112.1(1) ° O-Mo-O angles that are close to those reported for a $BaMoO_4$ ceramic prepared by conventional solid-sintering method [22]. Eight oxygen atoms, 4 at 2.741(1) and 4 at 2.777(1) Å from Ba, are arranged at the vertices of BaO_8 coordination polyhedra with $\bar{4}$ symmetry (Figure 1). The full CIF file is freely available with the CSD number 2112357 at the Cambridge Crystallographic Data Center [23].

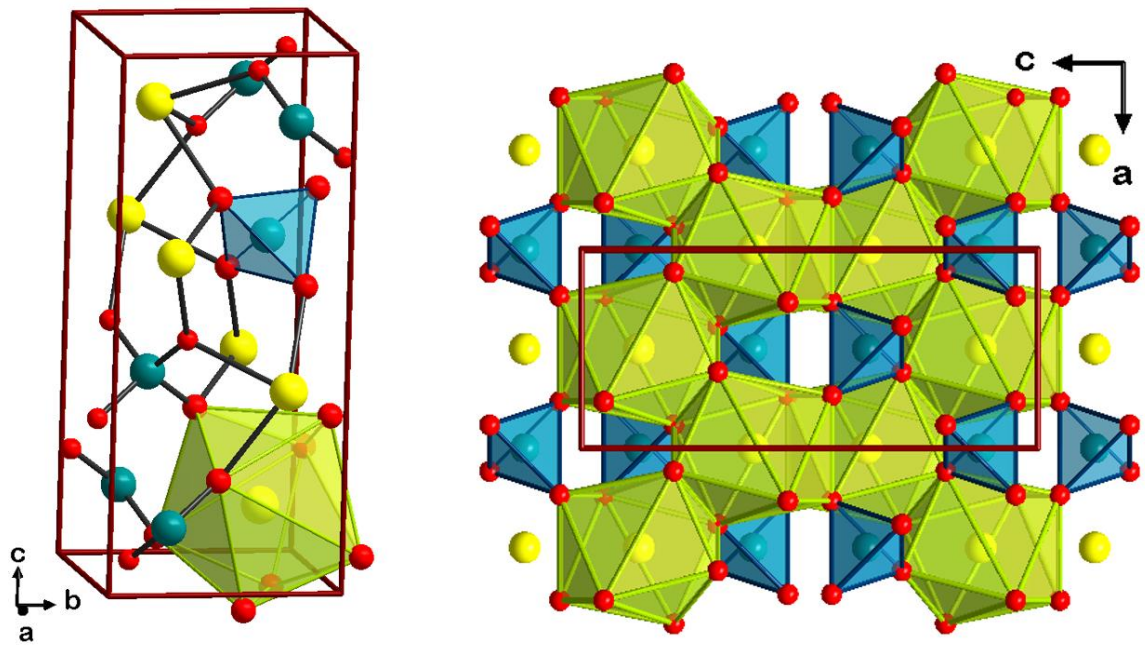

Figure 1. Representations of the scheelite-like $BaMoO_4$ structure with blue MoO_4 tetrahedra and green BaO_8 coordination polyhedra. The unit cell is drawn as brown lines. Yellow balls for Ba, red for O, and blue for Mo.

3.3. Single-crystal structure of $BaKYb(MoO_4)_3$

The main structural parameters and the X-ray data collection parameters are reported in Table 1 for the two barium molybdates.

Table 1. Crystal data, structure refinement, and data collection details

Formula	**$BaMoO_4$**	**$BaKYb(MoO_4)_3$**
	Lattice and symmetry	
Symmetry	tetragonal	monoclinic
Space group	*$I4_1/a$* (88)	*C2/c* (15)
Lattice dimensions (Å, °)	*a* = *b* = 5.5723(4)	*a* = 17.3517(5)
	c = 12.7954(9)	*b* = 12.1477(4)
		c = 5.2481(2)
		β = 105.344(2)
Lattice volume ($Å^3$)	397.30(6)	1066.78(6)
Z	4	4
Calculated density	6.307	5.164
	Data collection at 298 K	
Radiation, wavelength (Å)	Mo Kα, 0.71073	Mo Kα, 0.71073
θ range (°)	3.9-28.8	3.3-37.8
Absorption coefficient (mm^{-1})	13.03	16.19
	Full-matrix least-squares refinement on F^2	
Independent reflections	253 [R_{int} = 0.025]	2596 [R_{int} = 0.029]
Final indices [I > 2σ(I)] *R1*, *wR2*	0.0128, 0.0361	0.0152, 0.0333
R1, *wR2* (all data)	0.0137, 0.0364	0.0154, 0.0334
Density residuals ($e.Å^{-3}$)	0.60/−0.39	0.25/−1.15

The reflections initially collected for a crystal selected as a single crystal indicated the *I*-centering for a monoclinic cell with a = 5.2, b = 12.1, c = 16.4 Å, β = 92 ° but slight dispersion was noted in the diffraction images suggests twinning. Since the monoclinic angle does not deviate too much from 90 °, a two-fold rotation around any of the axes would lead to an almost perfect lattice overlay. Yet, a reasonable structural solution could be found after transformation into a monoclinic *C*-cell with a = 17.4, b = 12.1, c = 5.2 Å, β = 105 ° by applying the transformation matrix [$\bar{1}0\bar{1}010100$] to the data. The structure was finally confirmed by the full structural refinement to R1 = 1.52% using a new set of reflections collected later for a suitable single crystal, *C2/c*, a = 17.3517(5), b = 12.1477(4), c = 5.2481(2) Å, β = 105.344(2) °.

Among the ten independent positions, a general site 8*f* and a special site 4*e* were attributed to the most electropositive elements, a site 8*f* and a site 4*e* to molybdenum atoms, and the six remaining 8*f* sites to oxygen atoms. As the same contents are expected for K, Ba, and Yb, an atomic mixing must be considered on the two sites assigned to electropositive elements, Table 2.

Table 2. Atomic coordinates ($\times 10^4$) and equivalent isotropic displacement parameters (Å$^2 \times 10^3$)

Atom	**site**	**x**	**y**	**z**	**U_{eq}**
Yb	4*e*	0	6154(1)	2500	7(1)
Mo1	4*e*	0	1551(1)	2500	9(1)
Mo2	8*f*	1552(1)	3928(1)	3976(1)	8(1)
Ba/K	8*f*	3359(1)	3747(1)	752(1)	13(1)
O1	8*f*	394(1)	2350(1)	266(2)	14(1)
O2	8*f*	742(1)	4629(1)	1435(2)	11(1)
O3	8*f*	2059(1)	3019(1)	2461(2)	15(1)
O4	8*f*	786(1)	707(1)	4203(2)	19(1)
O5	8*f*	2723(1)	285(1)	3807(2)	16(1)

O6	8*f*	3912(1)	1850(1)	3965(2)	13(1)

With a higher symmetric environment and slightly shorter distances to surrounding oxygen atoms, the 4*e* site was found filled by ytterbium. Potassium and barium larger cations, with ionic radii of 1.42 and 1.51 Å, compared to 1.14 for Yb cation, are statistically mixed at the 8*f* position. Their fraction at this site freely refines, within the standard deviation limits, to equivalent amounts leading to the formula $Ba_{3.98}K_{4.02}Yb_{3.97}(MoO_4)_{12}$ in which the charge balance is almost perfectly fulfilled without any constrain to the final formula is $BaKYb(MoO_4)_3$. A bond valence sum analysis was performed using the most recently established parameters [24], available from IUCR resources [25]. This is an empirical way to estimate the oxidation state of a metal ion from its distances to surrounding ligands. It leads to valence numbers close to 6 for Mo and 3 for Yb and adds further weight to the complete ordering of the Yb atoms on the 4*e* site.

The Mo-O distances are in range1.732-1.866 Å and more precisely the tetrahedra with symmetry 2 are built around Mo atom at 4*e* site with 2 × 1.751(1) and 2 × 1.792(1) Å distances while a greater distortion is found at the tetrahedra formed around Mo at the 8*f* site (symmetry 1, distances 1.732(1), 1.754(1), 1.780(1) and 1.866(1) Å). The Yb atoms are surrounded by eight oxygen at 2.313(1)-2.405(1) Å within YbO_8 units while the Ba/K atoms have eight oxygen neighbors located at longer distances from 2.702(1) to 2.866(1) Å. The full CIF file with the CSD number 2112359 can be freely obtained from the Cambridge Crystallographic Data Center [23].

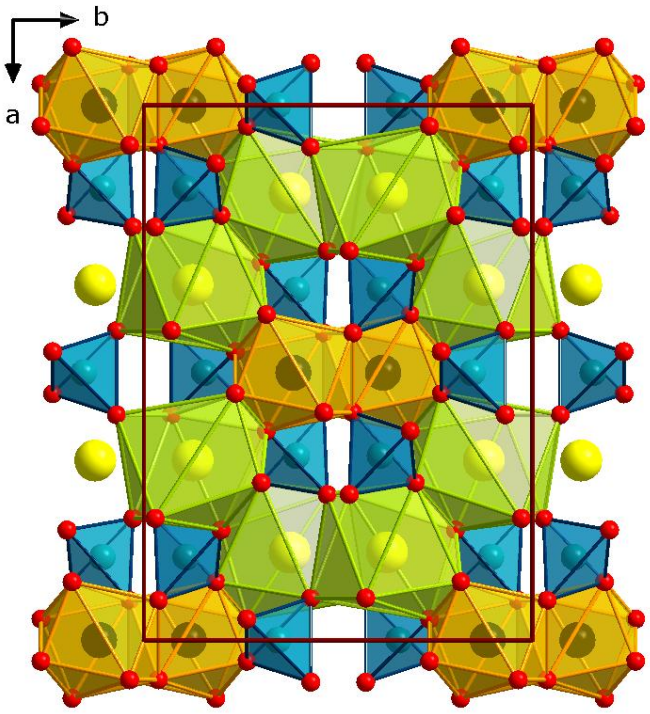

Figure 2. Representation of the structure of $BaKYb(MoO_4)_3$ with blue MoO_4 tetrahedra The unit cell is drawn as brown lines, the 8-vertex coordination polyhedra around Ba/K in green, and around Yb in orange. Yellow balls for Ba/K, red for O, blue for Mo, and brown for Yb.

Looking at the arrangement of polyhedra, the structure of $BaKYb(MoO_4)_3$ represented in Figure 2 bears a strong resemblance with that of $BaMoO_4$, which can be otherwise formulated $Ba_3(MoO_4)_3$, given in Figure 1. They both contain discrete MoO_4 tetrahedra having no common O, but sharing their four O vertices with the neighboring XO_8 units (X = Ba, K, or Yb). Instead, the XO_8 units are involved in chains of polyhedra (Figures 1 and 2) by sharing edges with neighboring analogs.

3.4 Common building blocks

$BaMoO_4$ and $BaKYb(MoO_4)_3$ structures are composed with the same building blocks represented in Figure 3 involving four MoO_4 tetrahedra around two cationic positions (separated by 4.24 Å in $BaMoO_4$).

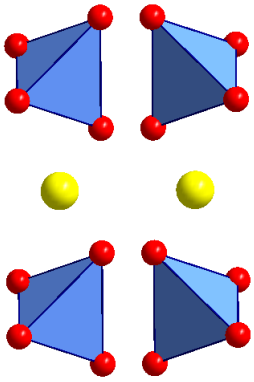

Figure 3. The common building blocks in the $Ba_3(MoO_4)_3$ and $BaKYb(MoO_4)_3$ structures. Blue MoO_4 tetrahedra and yellow balls for Ba/K, red for O.

However, the heterovalent substitution of two Ba in the $Ba_3(MoO_4)_3$ formula by one K and one Yb changes the symmetry so that a lower-symmetry and larger monoclinic unit cell is needed to describe the compound $BaKYb(MoO_4)_3$. Also, the cationic sites that were all equivalent in $BaMoO_4$, Figure 4a, are now divided into two categories, those filled with a Ba/K mixture and those filled with Yb, each of which being involved in a building block, Figure 4c. Depending on the nature of the cation, this causes local distortions of the building blocks that can be visualized with the greater spaces between the tetrahedra placed in the same layers as Yb at a = 0, ½ (see also in Figure 2) than the separation between tetrahedra placed in the same layers as Ba/K cations. The interatomic distances inside the Ba/K and Yb cationic pairs are measured respectively at 4.020(1) and 3.839(1) Å. Interestingly, the same building blocks are found in the structure of $LiYb(MoO_4)_2$ (Figure 4b) where the statistical Li/Yb atom distribution on the cationic sites allows the tetragonal symmetry to be maintained (with only a shift in the origin of the cell) [13]. Note that the distance between the cationic sites is here shortened to 3.77 Å.

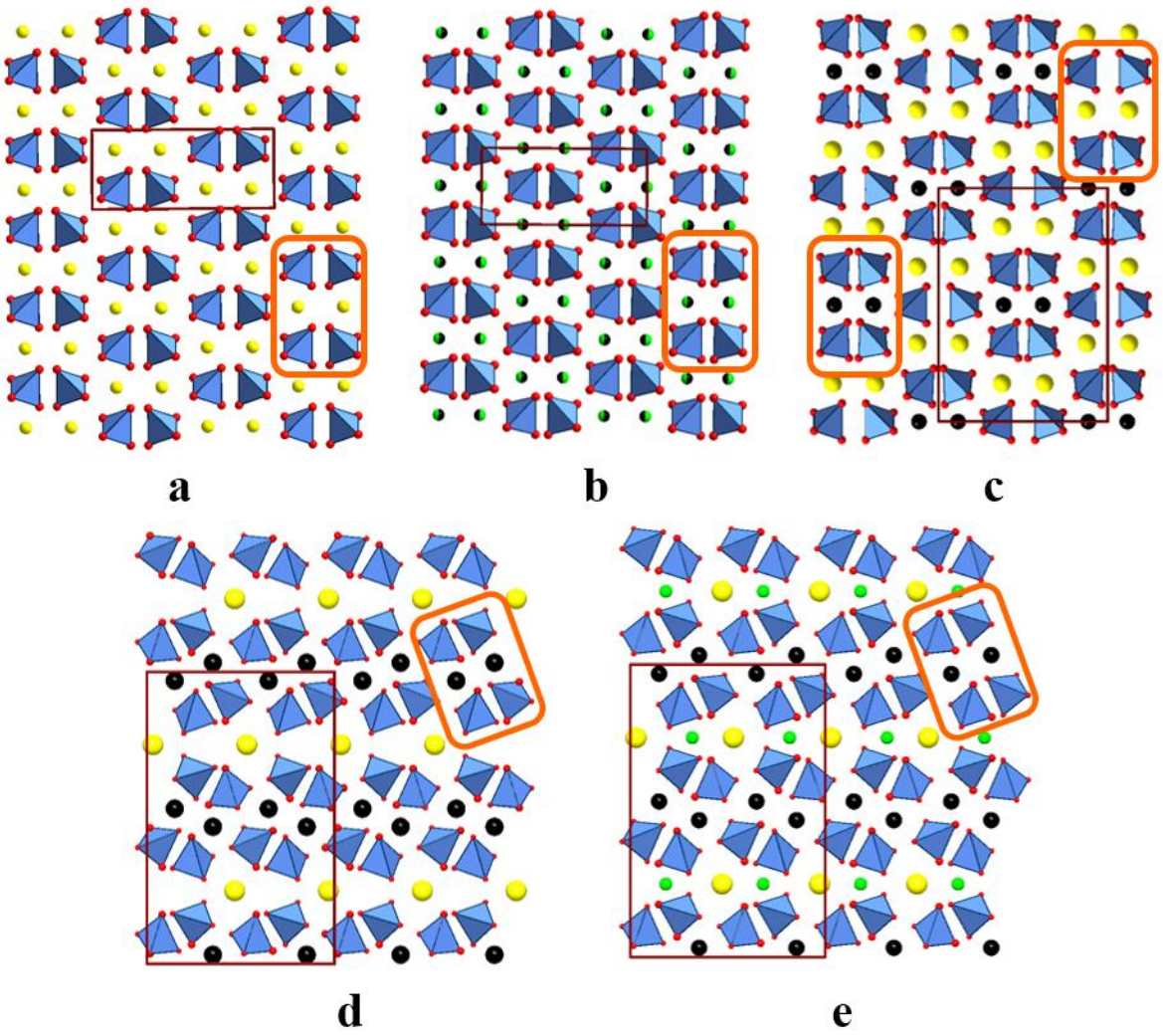

Figure 4. Respective arrangement of the 4×MoO_4 tetrahedra building blocks (highlighted with orange shapes) in some barium molybdates. Brown lines represent the unit cell limits. The representations were drawn from the structure data available in the literature. a- $Ba(MoO_4)$ [this work], b- $LiYb(MoO_4)_2$ [13], c- $BaKYb(MoO_4)_3$ [this work], d- $BaYb_2(MoO_4)_4$ [26], and e- $BaLi_{1.5}Gd_{1.4}Yb_{0.1}(MoO_4)_4$ [27]. Yellow balls for Ba/K, green for Li, black for Yb and red for O.

Going further in the structural comparison reveals some similarities with the arrangement of polyhedra in the two barium molybdates $BaYb_2(MoO_4)_4$ and $BaLi_{1.5}Gd_{1.4}Yb_{0.1}(MoO_4)_4$ reported in the Pearson Crystal database [19]. These two monoclinic isostructural compounds are also formed with similar building blocks around the Yb cations, alternately tilted on the left or tilted on the right in the successive layers (Figure 4d and 4e).

The barium ytterbium molybdate $BaYb_2(MoO_4)_4$ can be viewed as deriving from $BaMoO_4$ (or $Ba_4(MoO_4)_4$) by changing three Ba for two Yb and one vacancy and would be then formulated $Ba\square Yb_2(MoO_4)_4$. From there, the substitution of Yb for Li and Gd is almost entirely achieved in the molybdate $BaLi_{1.5}Gd_{1.4}Yb_{0.1}(MoO_4)_4$ with additional Li found on an "insertion" position. As the Li, Gd, and Yb atoms are statistically distributed in proportions 25:70:5 at two sites, this molybdate could be formulated $BaLi(Li/Gd/Yb)_2(MoO_4)_4$. The Yb to Yb distances within the Yb cationic pairs is 3.87 Å in these barium molybdates and the Li to Ba separation in the latter compound is 3.75 Å.

Figure 4 illustrates the role played by the nature, size, and distribution of the cations between the MoO_4 tetrahedra in the whole structure packing. Starting with $BaYb_2(MoO_4)_4$ and replacing the Yb atoms with Gd and Li atoms provides an isostructural arrangement where Gd is in place of Yb. For the heavy atoms Yb and Gd, there is little change in the covalent radii (1.94 and 1.79 Å) or even in the more appropriate Shannon effective ionic radii (0.868 and 0.938 Å) , and the smaller ionic radii of Li^+ (0.76 Å) allows lithium to take place at insertion positions [28]. On the contrary, the path from $BaYb_2(MoO_4)_4$ to $BaKYb(MoO_4)_3$ needs to change Yb atoms for larger Ba or K elements, whether one considers their covalent (2.17 and 2.27 Å) or ionic (1.37 and 1.35 Å) radii, and this cannot be achieved without a structural reorganization.

3.5. Vibrational properties

The unpolarized Raman scattering spectra were recorded at room temperature on the as-grown crystalline samples, Figure 5. It should be mentioned that no Raman band is observed in the frequency range beyond 1000 cm^{-1}.

Compared to the T_d symmetry of an isolated MoO_4 tetrahedron, the symmetry of $[MoO_4]^{2-}$ units with strong covalent bonds Mo-O is reduced to S_4 (or $\bar{4}$) point symmetry in the scheelite-type $BaMoO_4$ with tetragonal symmetry C_{4h}^6. This leads to a splitting of the degenerate vibrations due to the Crystal Field (CF) effect and Davydov Splitting (DS) [9]. The MoO_4 internal modes are

then identified as ν_1 (Ag), ν_3 (Bg and Eg) (stretching modes), ν_2 (Ag and Bg), and ν_4 (Bg and Eg) (bending modes) which are Raman-active vibration modes [1, 29]. The range of stretched vibrations of MoO_4 polyhedral is 700–1000 cm^{-1}. The narrowest and intensive line at 895 cm^{-1} is associated with antisymmetric Mo–O stretching vibrations into the MoO_4 tetrahedra, and attributed to the bond vibration line ν_1 (A_g) of $BaMoO_4$ crystal [1, 29]. The bands at 791 and 836 cm^{-1} are assigned to the ν_3 modes, and the frequencies of internal bending vibrations of MoO_4 tetrahedra are in the 300 - 400 cm^{-1} range as already reported [1, 29]. The external modes, called lattice phonon modes, correspond to the motion of the deltahedral [BaO_8] clusters and the rigid molecular unit and are present under 150 cm^{-1} [1, 29].

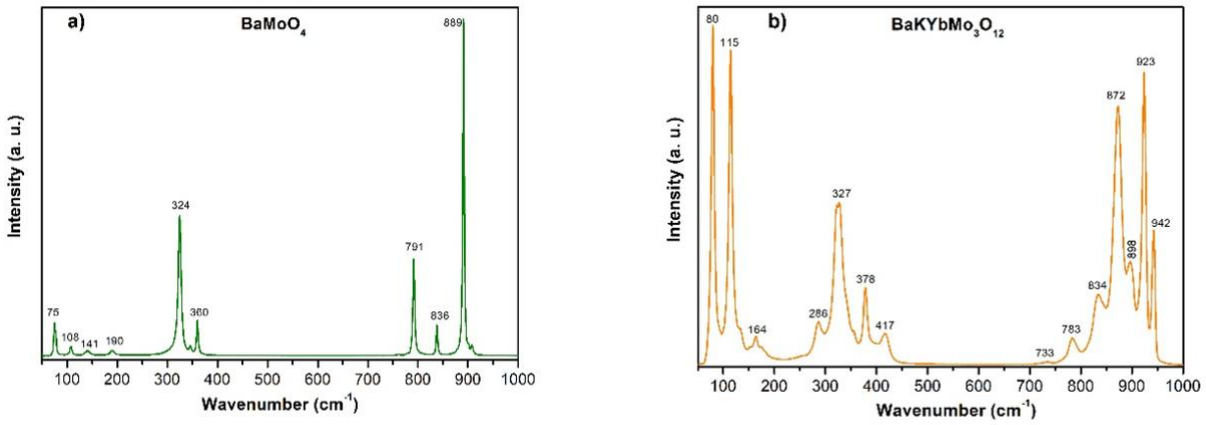

Figure 5. The Raman spectra in 50 - 1000 cm^{-1} range measured on the as-grown crystals of a) $BaMoO_4$ and b) $BaKYb(MoO_4)_3$.

The Raman spectrum for the $BaKYb(MoO_4)_3$ material presents three main segment bands between 50 and 200 cm^{-1}, 250 - 450 cm^{-1}, and 700 - 1000 cm^{-1}, Figure 5b. The maximum phonon frequency is 942 cm^{-1}. Compared to $BaMoO_4$, Figure 5a, the Raman spectrum of the ternary molybdate is composed of bands with larger width at half maximum in agreement with the existence of two independent crystallographic sites for Mo atoms in its disordered structure. It is interesting to remark the strong resemblance of the Raman spectrum recorded in the current

study for $BaKYb(MoO_4)_3$ with that reported for the yttrium homolog [30]. This was expected given the presumed isotypy of their structures (same lattice and symmetry), despite some differences in the atomic coordinates reported for $BaKY(MoO_4)_3$ [31]. However, no complete cif-file is available precluding further comparison with the Yb-based triple molybdate under study. We think that a transcription error in the atomic positions is at the origin of an erroneous description of this structure with two types of polyhedra, MoO_4 and MoO_6. Our diagnosis is confirmed in the recent paper giving both the Raman spectra and the structure of the yttrium molybdate described with only oxygen tetrahedra around Mo atoms [32].

In the monoclinic structure of $BaKYb(MoO_4)_3$, the Mo^{6+} ions coordinate with oxygen in isolated tetrahedral $(MoO_4)^{2-}$ polyhedra, which means that no Mo-O-Mo bridge is present in the structure. The complexity of the spectrum is well explained by the degeneracy removal of the stretching modes due to the symmetry lowering ($Td \rightarrow C_1$) of the distorted MoO_4 tetrahedra since four lines can be present in the symmetric stretching domain and up to 12 in the asymmetric range [33]. The bands in the range 250 - 450 cm^{-1} are assigned to the internal asymmetric and symmetric bending vibration δ(O-Mo-O) of the MoO_4 tetrahedra [12, 13, 33]. Below 200 cm^{-1}, the bands are due to external vibrations that involve the rotational and translational modes of the $(MoO_4)^{2-}$ anions and the translational modes of the cations [12, 13, 33].

3.6. Magnetic properties

The magnetization of the triple molybdate $BaKYb(MoO_4)_3$ was measured for a powdered sample placed in a constant magnetic field H of 0.5 T at temperatures ranging from 1.8 to 300 K. The magnetic susceptibility χ is defined as M/H. The electronic configuration of the paramagnetic Yb^{3+} isolated ion is [*Xe*] $4f^{13}$ and the effective magnetic moment μ_{eff} of Yb^{3+} is equal to 4.54 μ_B.

The normalized Yb molar dc magnetic susceptibility is temperature-dependent, as shown in Figure 6.

No anomaly is visible on the χ curve in the entire temperature range studied.

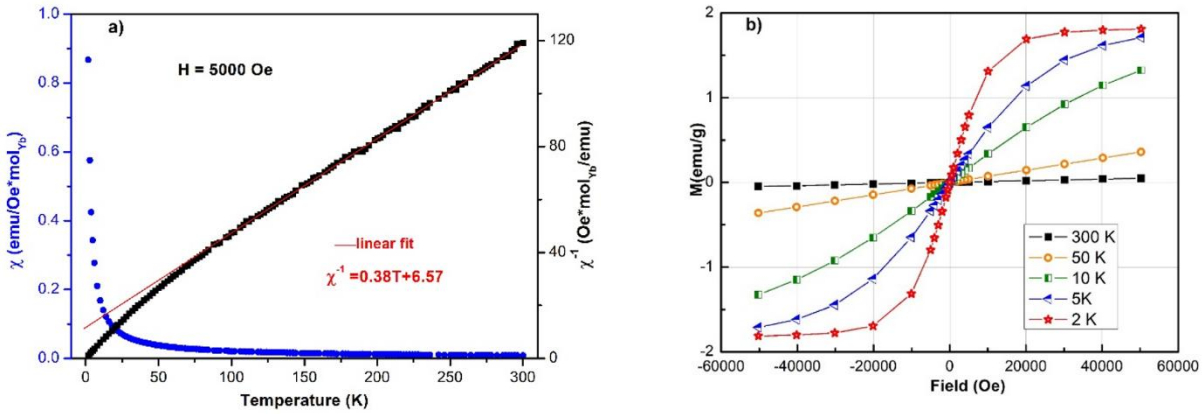

Figure 6. (a) Magnetic and inverse susceptibility χ of crushed $BaKYb(MoO_4)_3$ crystals in a constant H field as a function of the temperature, with a Curie-Weiss fit (red line) of the high-temperature data, (b) M-H curves recorded at different temperatures normalized by the mass.

From 300 K down to 75 K, the inverse magnetic susceptibility χ^{-1} is linear that characterizes a localized paramagnetic behavior, Figure 6a. The data obey a Curie-Weiss law $\chi_{mol} = C/(T-\theta p)$ with the least-squares parameters C = 2.63(1) emu.mol^{-1} (Curie constant) and $\theta p = -33.8$ K (paramagnetic Curie-Weiss temperature). The deviation from the Curie–Weiss law appears at 72 ± 2 K. The experimental effective magnetic moment μ_{eff} of 4.59(1) $\mu_{B/Yb}$, calculated for $BaKYb(MoO_4)_3$ from the Curie constant C and the equation $\mu_{eff} = (8\times C)^{1/2}$, is in good agreement with the value expected for μ_{eff} of the Yb^{3+} free-cation ($4f^{13}$, J = 7/2). The large negative value of θ_p (−33.8 K) suggests an antiferromagnetic exchange interaction between the Yb^{3+} magnetic moments in the low temperature range.

In the 1.8-75 K temperature range and for *H* = 5000 Oe, the inverse susceptibility data no longer follow a strict linear behavior with temperature. Such a deviation of the data from the expected

Curie-Weiss behavior for free ions would be rather assigned to the splitting of the J-multiplet ground state of the Yb^{3+} Kramers ion under the influence of the CF effect than to a magnetic order (no Néel temperature).

Figure 6b shows the field-dependent M-H curves registered for $BaKYb(MoO_4)_3$ for temperatures ranging from 2 K up to 300 K. The temperature variation was found to significantly impact the shape of the curves. As already observed for Yb-based molybdates, different magnetic regimes are observed [12, 13]. At T = 300 K, the normalized magnetization M is a linear function of the external alternating magnetic field H in good accordance with a paramagnetic behavior. At T = 2 K, the magnetization displays a large field dependence with a saturation zone starting from H = 20 kOe up to the highest applied magnetic field H = 50 kOe. The H strength is sufficient to magnetize the sample to saturation. This M-H curve shape could be attributed to an antiferromagnetic behavior between the Yb^{3+} magnetic moments.

4. Conclusion

The new $BaKYb(MoO_4)_3$ triple molybdate was obtained as transparent and colorless single crystals, using a high-temperature solution technique. The flux-grown material crystallizes in the monoclinic symmetry with the Mo^{VI} valence state and displays an ordered distribution of the Yb^{3+} cations on a C_2 symmetry position while the K^+ and Ba^{2+} are mixed at a general position. The Raman analysis confirms that the symmetry lowering around the Mo^{6+} position from $BaMoO_4$ to $BaKYb(MoO_4)_3$ leads to a degeneracy rise and thus to an increase of the number of bands assigned to the internal Mo-O vibrations of MoO_4 tetrahedra. Magnetic properties of $BaKYb(MoO_4)_3$ have been investigated from 1.8 to 300 K. The temperature-dependent magnetic susceptibility follows a Curie-Weiss law from 75 to 300 K, with a large negative paramagnetic constant θp of -33.8 K which may indicate an antiferromagnetic behavior between the Yb^{3+} ions

in the low temperature range. Therefore, an investigation of the magnetic interactions, and the magnetic unit cell, is needed to elucidate all interactions present.

Acknowledgments

The EDX experiments were conducted at the Plateau Technique Microscopie à Balayage at the IEM Institute in Montpellier, France. Raman and magnetic experiments were done at the Platform of Analysis and Characterization of the Pôle Chimie Balard in Montpellier, France. The single-crystal X-ray diffraction experiments were done using the technological resources of the X-ray and gamma-ray network of the University of Montpellier, France.

Funding information

Funding for this research was provided by the Ministry of Higher Education, Scientific Research and Innovation in France and the French National Center of Scientific Research (CNRS).

References

[1] Spontaneous Raman spectroscopy of tungstate and molybdate crystals for Raman lasers
T.T. Basiev, A.A. Sobol, Yu. K. Voronko, P.G. Zverev
Opt. Mater. 15 (2000) 205-216.
Doi: 10.1016/S0925-3467(00)00037-9

[2] Low-temperature flux growth of sulfates, molybdates, and tungstates of Ca, Sr, and Ba and investigation of doping with Mn^{6+}
Y.E. Romanyuk, D. Ehrentraut, M. Pollnau, S. Garcia-Revilla, R. Valiente
Appl. Phys. A 79 (2004) 613–618.
Doi: 10.1007/s00339-004-2555-8

[3] Synthesis and luminescence properties of BaMoO4:Sm3+ phosphors
Z. Xia, D. Chen.
J. Am. Ceram. Soc. 93 (2010) 1397-1401.
Doi: 0.1111/j.1551-2916.2009.03574.x

[4] Characteristic features of the crystal chemistry of lanthanide molybdates and tungstates
V. A. Efremov
Russ. Chem. Rev. 59(7) (1990) 627-642.
Doi: 10.1070/RC1990v059n07ABEH003547

[5] Mutual energy transfer luminescent properties in novel $CsGd(MoO_4)_2:Yb^{3+},Er^{3+}/Ho^{3+}$ phosphors for solid-state lighting and solar cells.
K. Li, R. van Deun
Phys.Chem.Chem.Phys. 21 (2019) 4746- 4754.
Doi: 10.1039/c8cp06538a

[6] The optical spectroscopy of lanthanides R^{3+} in $ABi(XO_4)_2$ (A= Li, Na; X= Mo, X) and $LiYb(MoO_4)_2$ multifunctional single crystals: Relationship with the structural local disorder.
C. Cascales, A. Méndez Blas, M. Rico, V. Volkov, C. Zaldo
Opt. Mater., 27 (2005) 1672-1680
Doi: 10.1016/j.optmat.2004.11.051

[7] $La_2(MoO_4)_3$@C as novel anode for lithium-ion battery: Structural and chemical evolutions upon electrochemical cycling.
Cheng Jiang, Tingting Liu, Runtian Zheng, Na Peng, Jundong Zhang, Xing Cheng, Haoxiang Yu, Miao Shui, Jie Shu.
Ceram. Int. 45, Issue 6 (2019) 7754-7760.
Doi:10.1016/j.ceramint.2019.01.079.

[8] Unveiling the Intercalation Mechanism in $Fe_2(MoO_4)_3$ as an Electrode Material for Na-Ion Batteries by Structural Determination
J. W. Heo, J. Hyoung, S.-T. Hong
Inorg. Chem. 57 (2018) 11901-11908.
Doi: 10.1021/acs.inorgchem.8b01244

[9] Growth and spectroscopy of orthorhombic $Yb:KY(MoO_4)_2$ laser crystal with a layered structure.
A. Volokitina, P. Loiko, J-M. Serres, X. Mateos, N. Kuleshov, V. Trifonov, A. Pavlyuk
J. Phys.: Conf. Series, 1410 (2019) 012149
Doi: 10.1088/1742-6596/1410/1/012149

[10] Double tungstate and molybdate crystals for laser and nonlinear optical applications
E.V. Zharikov, C. Zaldo, F. Diaz
MRS bulletin 34 (2009) 271-275.
Doi: 10.1557/mrs2009.78

[11] Crystal Growth and Optical and Spectroscopic Characterization of the Ytterbium-Doped Laser Molybdate $Yb{-}Li_3Gd_3Ba_2(MoO_4)_8$
A. García-Cortés, C. Cascales
Chem. Mater. 20 (2008) 3884–3891
https://doi.org/10.1021/cm703138x

[12] Growth, single-crystal structure, and magnetic properties of the double molybdate $KYb(MoO_4)_2$
P. Armand, C. Reibel, D. Granier, M. Tillard
J. Phys. Chem. Solids 154 (2021) 110023
Doi: 10.1016/j.jpcs.2021.110023

[13] Structure, vibrational and magnetic characteristics of $LiYbX_2O_8$ (X = W, Mo) single-crystals
P. Armand, D. Granier, C. Reibel, L. Daenens, M. Tillard
J. Alloys Compd. 884 (2021) 161074
Doi: 10.1016/j.jallcom.2021.161074

[14] CrysAlis'Red software package, Oxford diffraction Ltd, Abingdon, United Kingdom, 2004.

[15] Bruker, APEX3. Version 2017.3-0, Bruker AXS, Inc., Madison, Wisconsin, USA, 2017

[16] Crystal structure refinement with *SHELXL*
G. M. Sheldrick
Acta Crystallogr. C71 (2015) 3-8
Doi: 10.1107/S2053229614024218

[17] SHELXT - Integrated space-group and crystal-structure determination
G. M. Sheldrick
Acta Crystallogr. A71 (2015) 3-8
Doi: 10.1107/S2053273314026370

[18] Diamond - Crystal and Molecular Structure Visualization
Crystal Impact
H. Putz, K. Brandenburg GbR, Kreuzherrenstr. 102, 53227 Bonn, Germany
http://www.crystalimpact.com/diamond

[19] Pearson's Crystal Data: Crystal Structure Database for Inorganic Compounds,
P. Villars, K. Cenzual
ASM International, Materials Park, Ohio, USA (Release 2009/10)

[20] Crystal structures of Ba molybdate and Ba tungstate
T. I. Bylichkina, L. I. Soleva, E. A. Pobedimskaya, M. A. Porai Koshits, N. S. Kurnakov, N. V. Belov.
Sov. Phys. Crystallogr. 15 (1970) 130-131

[21] Structural Disorder in $AMoO_4$ (A = Ca, Sr, Ba) Scheelite Nanocrystals
F. A. Rabuffetti, S. P. Culver, L. Suescun, R. L. Brutchey.
Inorg. Chem. 53 (2014) 1056-1061.
Doi: 10.1021/ic4025348

[22] Phonon characteristics and dielectric properties of $BaMoO_4$ ceramic
En-Cai Xiao, Jianzhu Li, Jing Wang, Chao Xing, Mei Guo, Hengyang Qiao, Qing Wang, Ze-Ming Qi, Gang Dou, Feng Shi.
J. Mater. 4 (2018) 383e389.
Doi: 10.1016/j.jmat.2018.08.004

[23] http://www.ccdc.cam.ac.uk/conts/retrieving.html (or from the CCDC, 12 Union Road, Cambridge CB2 1EZ, UK; Fax: +44 1223 336033; E-mail: deposit@ccdc.cam.ac.uk).

[24] Comprehensive derivation of bond-valence parameters for ion pairs involving oxygen
O.C. Gagne and F.C. Hawthorne
Acta Crystallogr. B71 (2015) 562-578.

Doi: 10.1107/S2052520615016297

[25] https://www.iucr.org/resources/data/datasets/bond-valence-parameters

[26] Zwei Beispiele für partielle und totale Defekte im Ba $Ln_2Mo_4O_{16}$-Typ: $BaCu_{0.41}Z_{0.59}Pr_2Mo_4O_{16}$ und $BaZYb_2Mo_4O_{16}$
S. Gallinat, H. K. Müller Buschbaum
Z. Naturforsch. B (1996) 51, 85-89
Doi: 10.1515/znb-1996-0116

[27] Crystal Growth and Optical and Spectroscopic Characterization of the Ytterbium-Doped Laser Molybdate Yb-$Li_3Gd_3Ba_2(MoO_4)_8$
A. Garcia Cortes, C. Cascales
Chem. Mater. (2008) 20, 3884-3891
Doi: 10.1021/cm703138x

[28] Revised Effective Ionic Radii and Systematic Studies of Interatomic Distances in Halides and Chalcogenides
R. D. Shannon
Acta Cryst. A32 (1976) 751-767.
Doi: 10.1107/S0567739476001551

[29] Sonochemical synthesis of $MMoO_4$ (M = Ca, Sr and Ba) nanocrystals
T. Thongtem, A. Phuruangrat, S. Thongtem
J. Ceram. Process. Res. 9 (2008) 189-191.

[30] Up-conversion luminescence and optical temperature sensing properties in novel $KBaY(MoO_4)_3$:Yb^{3+},Er^{3+} materials for temperature sensors
K. Li, D. Zhu, H. Lian
J. Alloys Compds 816 (2020) 152554
Doi: 10.1016/j.jallcom.2019.152554

[31] Assessment of structure and spectral characteristics of new laser crystal Nd^{3+}:$KBaY(MoO_4)_3$
Yi Yu, Yisheng Huang, Lizhen Zhang, Zhoubin Lin, Guofu Wang
J. Alloys Compds 651 (2015) 164-169
Doi: 10.1016/j.jallcom.2015.08.078

[32] $KBaY(MoO_4)_3$:Er^{3+}/Yb^{3+}-an Erbium/Ytterbium-Codoped Upconversion Phosphor in the K_2MoO_4–$BaMoO_4$–$Y_2(MoO_4)_3$ System
N.M. Kozhevnikova
Inorganic Materials 57(6):614-619
Doi: 10.1134/S0020168521060066

[33] Exploration of structural, vibrational and spectroscopic properties of self-activated orthorhombic double molybdate $RbEu(MoO_4)_2$ with isolated MoO_4 units
V. V. Atuchin, A. S. Aleksandrovsky, B. G. Bazarov, J. G. Bazarova, O. D. Chimitova, Y. G. Denisenko, T. A. Gavrilova, A. S. Krylov, E. A. Maximovskiy, M. S. Molokeev, A. S. Oreshonkov, A. M. Pugachev, Ni. V. Surovtsev
J. Alloys Compd. 785 (2019) 692-697.

Doi: 10.1016/j.jallcom.2019.01.013